A Two-Step K-Ar Experiment on Mars: Dating the Diagenetic Formation of Jarosite from Amazonian Groundwaters

Journal Item

AGU PUBLICATIONS

JGR

Journal of Geophysical Research: Planets

RESEARCH ARTICLE
10.1002/2017JE005445

Key Points:
- A third radiometric age dating experiment has been conducted on Mars
- The model formation age of plagioclase is greater than 4 Ga, while the model age for jarosite is less than 3 Ga
- The young jarosite age suggests the presence of liquid water in Gale Crater during the Amazonian period, most likely in the subsurface

Supporting Information:
- Supporting Information S1

Correspondence to:
P. E. Martin,
pmmartin@caltech.edu

Citation:
Martin, P. E., Farley, K. A., Baker, M. B., Malespin, C. A., Schwenzer, S. P., Cohen, B. A., … Navarro-González, R., (2017). A two-step K-Ar experiment on Mars: Dating the diagenetic formation of jarosite from Amazonian groundwaters. *Journal of Geophysical Research: Planets*, *122*, 2803–2818. https://doi.org/10.1002/2017JE005445

Received 12 SEP 2017
Accepted 27 NOV 2017
Accepted article online 5 DEC 2017
Published online 20 DEC 2017

A Two-Step K-Ar Experiment on Mars: Dating the Diagenetic Formation of Jarosite from Amazonian Groundwaters

P. E. Martin[1], K. A. Farley[1], M. B. Baker[1], C. A. Malespin[2], S. P. Schwenzer[3], B. A. Cohen[2], P. R. Mahaffy[2], A. C. McAdam[2], D. W. Ming[4], P. M. Vasconcelos[5], and R. Navarro-González[6]

[1]Division of Geological and Planetary Sciences, California Institute of Technology, Pasadena, CA, USA, [2]NASA Goddard Space Flight Center, Greenbelt, MD, USA, [3]Department of Physical Sciences, Open University, Milton Keynes, UK, [4]NASA Johnson Space Center, Houston, TX, USA, [5]School of Earth Sciences, University of Queensland, Brisbane, Queensland, Australia, [6]Instituto de Ciencias Nucleares, Universidad Nacional Autónoma de México, Ciudad Universitaria, México City, Mexico

Abstract Following K-Ar dating of a mudstone and a sandstone, a third sample has been dated by the Curiosity rover exploring Gale Crater. The Mojave 2 mudstone, which contains relatively abundant jarosite, yielded a young K-Ar bulk age of 2.57 ± 0.39 Ga (1σ precision). A two-step heating experiment was implemented in an effort to resolve the K-Ar ages of primary and secondary mineralogical components within the sample. This technique involves measurement of ^{40}Ar released in low-temperature (500°C) and high-temperature (930°C) steps, and a model of the potassium distribution within the mineralogical components of the sample. Using this method, the high-temperature step yields a K-Ar model age of 4.07 ± 0.63 Ga associated with detrital plagioclase, compatible with the age obtained on the Cumberland mudstone by Curiosity. The low-temperature step, associated with jarosite mixed with K-bearing evaporites and/or phyllosilicates, gave a youthful K-Ar model age of 2.12 ± 0.36 Ga. The interpretation of this result is complicated by the potential for argon loss after mineral formation. Comparison with the results on Cumberland and previously published constraints on argon retentivity of the individual phases likely to be present suggests that the formation age of the secondary materials, correcting for plausible extents of argon loss, is still less than 3 Ga, suggesting post-3 Ga aqueous processes occurred in the sediments in Gale Crater. Such a result is inconsistent with K-bearing mineral formation in Gale Lake and instead suggests postdepositional fluid flow at a time after surface fluvial activity on Mars is thought to have largely ceased.

1. Introduction

The surface regions of Mars and their associated geologic features are divided into three major epochs: the Noachian (4.1–3.7 Ga), the Hesperian (3.7–3.1 Ga), and the Amazonian (3.1 to present) (Hartmann & Neukum, 2001; Nimmo & Tanaka, 2005). The Noachian is characterized by abundant surface water, illustrated by the presence of phyllosilicates and high-drainage-density valley networks (e.g., Ehlmann et al., 2011; Fassett & Head, 2008). A relative increase in the proportions of sulfates and other evaporite minerals, along with the lack of highly dissected drainage networks, in Hesperian-aged terranes suggest a large-scale desiccation of Mars (Bibring et al., 2006). This overall drying trend continued in the Amazonian, with liquid water playing no apparent major role in generating or altering large-scale features of the Martian surface during this time period. Understanding the absolute and relative timing of these geomorphic and mineralogical features is critical to a complete understanding of the planet's evolution. However, the ages of Mars's epochs are based on cratering chronology and are accordingly subject to limitations and uncertainties inherent to that technique (e.g., Hartmann, 2005; Hartmann & Daubar, 2017; Hartmann & Neukum, 2001; McEwen et al., 2005; Robbins et al., 2014).

Although the Curiosity rover was not designed to implement the K-Ar method, by combining the capabilities of the Alpha Particle X-ray Spectrometer (APXS), CheMin, and Sample Analysis at Mars (SAM) instruments on board the rover, in situ radiometric dating of Martian materials by the K-Ar method is possible (Farley et al., 2014), albeit with analytical uncertainties far larger than those routinely obtained in terrestrial labs. The results of Farley et al. (2014) and Vasconcelos et al. (2016) represent the first attempts at off-planet radiometric geochronology. A K-Ar bulk age of 4.21 ± 0.35 Ga (1σ) was obtained from the Cumberland sample (Farley et al., 2014), drilled from the Sheepbed lacustrine mudstone in Gale Crater. This age is consistent with crater-counting results from nearby terranes (Le Deit et al., 2012) and the expected ancient age of igneous

materials on Mars, suggesting that the technique successfully retrieved the formation age of minerals in the sample. A second geochronology experiment was undertaken on the Windjana sandstone in the Kimberly formation; this experiment was clearly unsuccessful because it resulted in extremely variable and young K-Ar ages of 627 ± 50 Ma and 1710 ± 110 Ma on separate aliquots of the same sample (Vasconcelos et al., 2016). The failure of this second experiment has been attributed to incomplete argon extraction due to a combination of the larger grain size of the material sampled at Windjana compared to that of Cumberland, as well as the extraordinary abundance of the highly argon-retentive mineral sanidine (~20 wt %) in the Windjana sample.

The mudstone sample Mojave 2, drilled later in the mission in the Pahrump Hills, was found to contain several weight percent jarosite [$KFe_3(SO_4)_2(OH)_6$], making it the most jarosite-rich sample yet discovered by Curiosity (Rampe et al., 2017). Like many other samples measured by CheMin, Mojave 2 also contains phyllosilicates and an amorphous component (Rampe et al., 2017). As jarosite is formed by interaction with water (as are the phyllosilicates and possibly the amorphous materials), the Mojave 2 sample potentially offers an opportunity to investigate the timing of aqueous interaction with the sediments in Gale Crater relative to the formation of the potassium-containing detrital igneous grains (i.e., feldspar and any glass present) in those sediments. A unique aspect of the current work is an attempt to separate the ages of these two components. Jarosite has been shown to be suitable for K-Ar dating (Vasconcelos et al., 1994) and releases argon at temperatures below 500°C (Kula & Baldwin, 2011). In contrast, plagioclase retains the vast majority of its argon to above 500°C (e.g., Bogard et al., 1979; Cassata et al., 2009). To take advantage of this differential Ar release, a two-step heating methodology was devised and applied to Mojave 2; stepped heating experiments are a standard technique in noble gas geochronology used to resolve ages of various components in single samples. Such a two-step measurement was not attempted for the Cumberland sample to allow method development with a simpler analytical protocol; two-step heating for the Windjana sample was not attempted due to the small amount of potassium inferred to be held in its secondary phases. The phases present in Mojave 2 cluster conveniently by formation mechanism and argon release temperature: the low-temperature step should yield information about the formation and preservation of minerals associated with water in the sample (i.e., secondary components), while the high-temperature step should date detrital components only.

2. Sample and Methodology

2.1. Sample Description

The Mojave 2 drill hole is located stratigraphically low in the Pahrump Hills locality, which is in the Murray mudstone formation, at the base of Mount Sharp. The Pahrump Hills are ~13 m thick, representing the lowermost 10% of the Murray formation (Grotzinger et al., 2015). The Murray is a deposit of mudstone and fine-grained sandstone with millimeter-scale lamination interpreted to represent the distal lacustrine sediment deposited in the lake once contained in Gale Crater. Mojave 2 is located within a finely laminated mudstone in the Pahrump Hills, with a grain size too small to be resolved by the Mars Hands Lens Imager (MAHLI) (<60 μm; Grotzinger et al., 2015). These fine-grained sediments interfinger with the coarser-grained deltaic sediments, which comprise the lower Bradbury group (Grotzinger et al., 2015). The coarsening-upward nature of the Pahrump Hills sequence indicates fluvio-deltaic progradation over the older lacustrine mudstone deposits (Grotzinger et al., 2015).

Diagenetic features have been observed in the Pahrump Hills and in association with the Mojave 2 target specifically (Gellert et al., 2015; Grotzinger et al., 2015; McBride et al., 2015; Nachon et al., 2017; Schieber et al., 2015). Lenticular crystal laths, lighter in color than the host rock, comprise ~30% of the substrate in the brushed Mojave 2 target (Figure 1; McBride et al., 2015; Schieber et al., 2015). Their presence in broken pieces of outcrop show that these features extend vertically into the bedrock, implying that they are not simply a surface feature (Grotzinger et al., 2015). On the basis of morphology, these lenticular forms have been suggested to be gypsum crystals, which, in terrestrial environments, form in saline mudflats and ephemeral lakes (Mees et al., 2012; Schieber et al., 2015). Given the lack of mineralogical (CheMin) or chemical (APXS) evidence for calcium sulfates in the Mojave 2 sample, it is possible that these crystal laths formed syndepositionally with the Murray mudstone and were later redissolved by postdepositional fluid flow, forming pseudomorphs of unknown composition (L. Kah, personal communication, 2017).

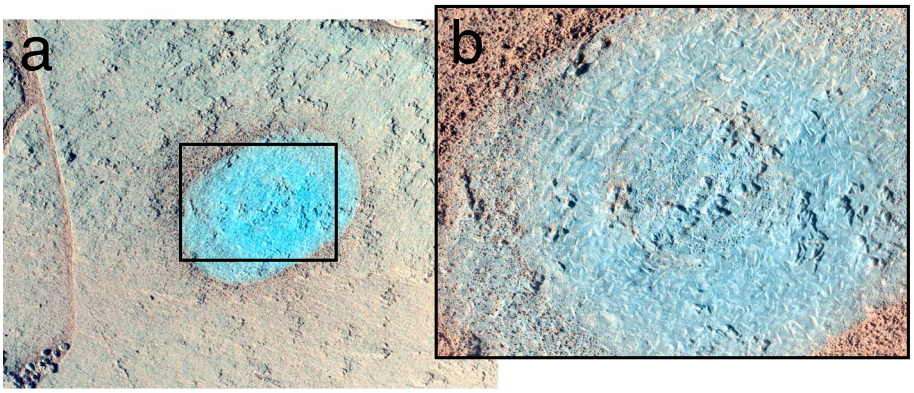

Figure 1. MAHLI images of (a) the brushed Mojave 2 surface, showing pronounced crystal laths, and (b) a magnification of the image in the area denoted by the black rectangle. The brushed area is approximately 4 cm across along the short axis. The color has been stretched to increase contrast.

Drilling followed standard MSL procedures: a 5 cm deep hole was drilled, and rock from below 1.5–2 cm depth was delivered to the CHIMRA unit on board Curiosity (Sunshine, 2010). The rock cuttings were sieved to <150 μm for delivery to SAM and CheMin (Anderson et al., 2012; Mahaffy et al., 2012).

2.2. Sample Chemistry and Mineralogy

The mineralogy of Mojave 2 includes plagioclase and jarosite and no detectable sanidine (~1 wt % detection limit (Vaniman et al., 2014); the full mineralogy is listed in Table 1). This mineral assemblage paradoxically suggests both oxidizing (hematite) and reducing (magnetite) environments, as well as acidic (jarosite) and neutral (apatite) conditions. This juxtaposition could imply a postdepositional acidic, oxidizing fluid flowed through the Pahrump Hills area, possibly forming the jarosite (Rampe et al., 2017). Mojave 2 also contains an amorphous phase making up over 50 wt % of the total sample (Rampe et al., 2017). A comparison to the apparently successful geochronology experiment on Cumberland reveals that the only major difference in mineralogy between the two samples is the presence of jarosite in Mojave 2, which is known to be amenable to argon extraction at relatively low temperatures. In contrast with the failed run at Windjana on the other hand, the lack of coarse-grained sanidine in Mojave 2 eliminates this potential difficulty with argon extraction.

Table 1
Mineralogy of Samples Used for Geochronology by Curiosity

Mineral	Mojave 2[a]	Windjana[b]	Cumberland[c]
Plagioclase	**23.5 ± 1.6**	**3.0 ± 0.3**	**22.2 ± 1.3**
Sanidine	**-**	**21.0 ± 3.0**	**1.6 ± 0.8**
Olivine	0.2 ± 0.8	4.7 ± 1.0	0.9 ± 0.45
Augite	2.2 ± 1.1	20 ± 0.3	4.1 ± 1.0
Pigeonite	4.6 ± 0.7	11 ± 0.2	8.0 ± 2.0
Orthopyroxene	-	-	4.1 ± 1.0
Magnetite	3.0 ± 0.6	12 ± 0.2	4.4 ± 1.1
Hematite	3.0 ± 0.6	0.6 ± 0.4	0.7 ± 0.35
Anhydrite	-	0.4 ± 0.3	0.8 ± 0.4
Bassanite	-	0.5 ± 0.4	0.7 ± 0.35
Quartz	0.8 ± 0.3	-	0.1 ± 0.1
Jarosite	**3.1 ± 1.6**	**-**	**-**
Fluorapatite	1.8 ± 1.0	0.8 ± 0.8	-
Ilmenite	-	0.8 ± 0.5	0.5 ± 0.5
Akaganeite	-	0.2 ± 0.2	1.7 ± 0.85
Halite	-	-	0.1 ± 0.1
Pyrrhotite	-	0.3 ± 0.3	1.0 ± 0.5
Phyllosilicate	**4.7 ± 2.4**	**10 ± 0.2**	**18 ± 9**
Amorphous	**53 ± 15**	**15 ± 0.3**	**31 ± 19**

Note. Phases potentially containing significant potassium are in bold. See references for discussions of reported uncertainties.
[a]Rampe et al. (2017). [b]Treiman et al. (2016). [c]Vaniman et al. (2014).

The chemical composition of Mojave 2 was measured several times by the APXS instrument: the surface of Mojave 2 after the dust removal tool was applied to the surface, tailings from a preliminary "minidrill" of the Mojave 2 outcrop, the drill tailings from the full drill, the dump pile from before sieving was completed (unsieved), and the dump pile discarded after sieving (sieved to <150 μm) and delivery to the SAM and CheMin instruments; these measurements yielded K_2O contents of 0.69, 0.74, 0.63, 0.73, and 0.73 wt %, respectively. Of the available measurements, the presieve and postsieve dump piles are the most closely related to the K_2O content of the Mojave 2 sample measured by SAM, because they consist of the same material taken from below the 1.5–2 cm depth during drilling, while the other measurements targeted materials which were not ingested by the rover. The fact that the K_2O measurements of the presieve and postsieve sample are identical adds confidence in this measured value. The full chemistry of the postsieve dump pile is shown in Table 2.

2.3. Release Temperatures

To correlate the ^{40}Ar releases in each temperature step (<500°C and 500–930°C) with the component of the sample containing the associated parent ^{40}K, the temperature step in which each potassium-bearing material releases Ar must be established. Of the minerals in

Table 2
APXS Results From Mojave 2

	Chemistry (wt %)
SiO_2	49.48
TiO_2	1.19
Al_2O_3	11.43
FeO	16.11
MnO	0.40
MgO	4.55
CaO	4.33
Na_2O	3.01
K_2O	0.73
P_2O_5	1.29
Cr_2O_3	0.37
Cl	0.43
SO_3	6.27
Ni (ppm)	1032
Zn (ppm)	2204
Br (ppm)	65

Note. Measured on the post-sieve dump pile. Accuracy relative to calibration is 15% of the absolute value (R. Gellert, personal communication, 2017).

Mojave 2, plagioclase, jarosite, phyllosilicates (e.g., illite), the amorphous phase(s), and possibly pyroxene are the only components likely to contain significant proportions of the total potassium. Pyroxenes release argon at very high temperatures (Cassata et al., 2011). However, the median K_2O content of over a thousand microprobe analyses of pyroxenes in Martian meteorites with nonzero K_2O values is ~0.02 wt % (references given in the supporting information), indicating that the ~6.8 wt % of pyroxene in Mojave 2 plays no role in the K-Ar characteristics of this bulk-rock analysis. Plagioclase hosts potassium (see section 3.1 below) and is known to release the vast majority of its argon in excess of 500°C (Bogard et al., 1979; Cassata et al., 2009), so it will degas almost entirely in the high-temperature step. Indeed, complete Ar degassing from plagioclase might be expected to require temperatures higher than the 930°C achieved in the SAM oven. Based on the very old age of 4.21 ± 0.35 Ga measured on the Cumberland mudstone, complete (or near-complete) extraction of Ar from feldspar was apparently achieved (Farley et al., 2014). It is possible that the small grain size of the mudstone and/or flux melting associated with volatile-bearing minerals in the rock aid in the release of Ar. The similarities in grain size and mineralogy between Mojave 2 and Cumberland suggest that near-complete Ar release from plagioclase in Mojave 2 might be expected as well. Jarosite begins to break down structurally at ~300°C, implying that Ar release occurs via disruption of the mineral lattice (as opposed to diffusion) well below the first temperature step cutoff of 500°C (Kula & Baldwin, 2011). In Ar-Ar dating experiments, illite and other clays have been shown to release >95% of their total Ar content below 500°C (Evernden et al., 1960; Hassanipak & Wampler, 1996). Illite argon release may also proceed by structural changes during dehydroxylation (Halliday, 1978), suggesting that behavior similar to jarosite might be expected.

Characterizing the expected Ar release temperatures for the amorphous fraction is more complex, since the phase or phases that host potassium in this material are uncertain, even though the amorphous fraction contains a nontrivial fraction of the potassium in Mojave 2 (see section 3.1 for discussion). Likely constituents of the amorphous fraction such as nanophase iron oxide, hissingerite, and allophane are devoid of potassium. Glass is unlikely to be present in Mojave 2 (see section 3.1.1) but would, if present, likely contain at least some potassium and release its argon mostly in the high-temperature step (Gombosi et al., 2015). More speculatively, potassium in the amorphous fraction may be carried by X-ray amorphous salts that would likely release Ar in the low-temperature step. As an example, the common K-bearing salt KCl (sylvite) releases Ar at temperatures <500°C (Amirkhanoff et al., 1961). Similarly, if any potassium-containing salts in Mojave 2 are hydrated, they could potentially behave in a similar manner to jarosite, breaking down via dehydration and releasing argon due to crystallographic shifts at <500°C (e.g., ~255°C for the common K-bearing sulfate polyhalite [$K_2Ca_2Mg(SO_4)_4{\cdot}2H_2O$]; Leitner et al., 2014). The assumption that any salts present would likely release Ar in the low-temperature step is also supported by the fact that they must be amorphous or nanocrystalline (≲500 unit cells) to avoid detection by CheMin. The tiny grain size and/or lack of large-scale crystalline order might further decrease the argon release temperatures of these materials.

To summarize, Ar in the high-temperature step will be strongly dominated by plagioclase, a detrital igneous mineral. In contrast, the low-temperature step will carry Ar from jarosite and possibly from nanocrystalline salts and clays. Jarosite and any salts in Mojave 2 are almost certainly diagenetic and/or authigenic (Rampe et al., 2017) and clays measured in earlier samples at Gale Crater appear to be authigenic (Bristow et al., 2015). Thus, the two-step experiment may isolate the K-Ar age of the detrital igneous components from the K-Ar age of fluid-associated low-temperature diagenetic/authigenic phases.

2.4. Noble Gas Extraction

Samples were delivered to preconditioned quartz cups in the SAM instrument prepared by the same method described by Ming et al. (2014). A portioning tube of known volume (76 mm^3) was used to

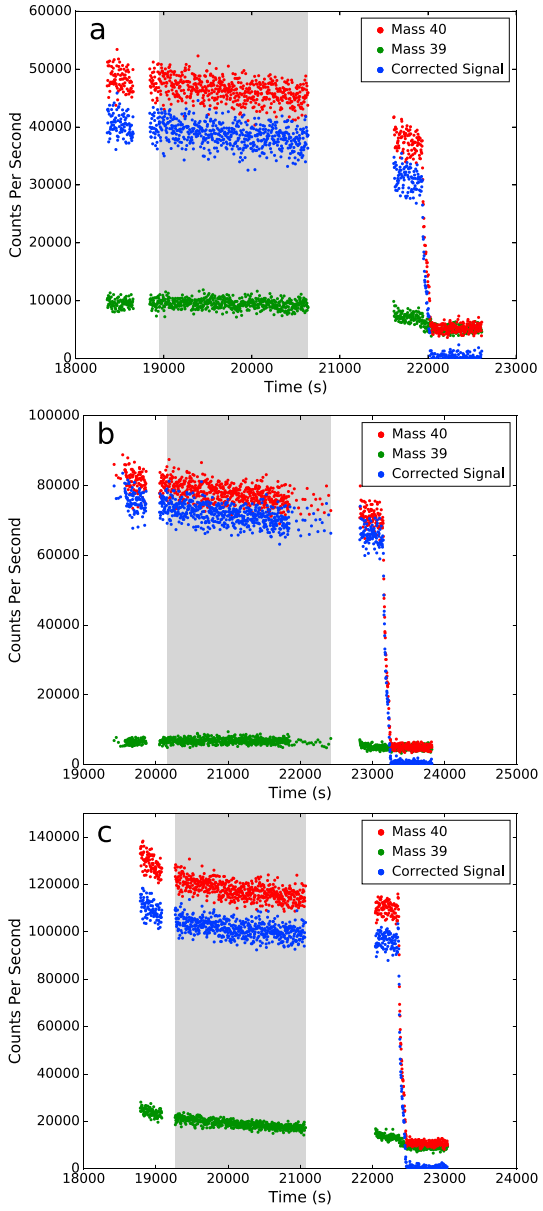

Figure 2. High-sensitivity mode and background measurement gas traces from (a) the high-temperature step of the failed run, (b) the high-temperature step of the successful run, and (c) the low-temperature step of the successful run. The stable (i.e., least sloped) portion of the runs are highlighted with the gray bar. Corrected Signal points are discussed in section 2.5.

pour sample into a funnel that delivered the powder to the SAM instrument. The exact amount of sample delivered is not directly measured. Rather, a model is used to describe the most likely amount transferred (Farley et al., 2014). Three separate aliquots of Mojave 2 were delivered to the SAM instrument to facilitate multiple independent measurements: two triple-portion aliquots (135 ± 18 mg each, all reported uncertainties are 1σ) were used for noble gas geochronology experiments, and one single-portion aliquot (45 ± 6 mg) was used in an evolved gas analysis (EGA; Sutter et al., 2017). While the first triple-portion aliquot was deposited in a pristine quartz cup, the second was deposited on top of the residue of the single-portion aliquot (i.e., into the same sample cup already used for EGA). It is possible that some ^{40}Ar could be retained by this single portion through the EGA heating process and then released during the high-temperature step of the noble gas experiment. Because the aliquot previously analyzed during EGA is one third of the mass of the aliquot used for noble gas measurement and because EGA reaches temperatures similar to those achieved in noble gas extraction, we consider the total effect of this potential extraneous argon release to be negligible.

After delivery, each sample was prepared for noble gas measurements by conducting a "boil-off" stage, where the sample was heated gradually over 26 min to a maximum target temperature of ~150°C under He flow to drive off adsorbed volatiles, which are mostly composed of residual derivatizing agent in the SAM vacuum system or adsorbed on the sample (Freissinet et al., 2015; Glavin et al., 2013). After boil off, the first step was performed by heating the sample monotonically to ~500°C over approximately 1 h, targeting phases that release argon at low temperatures. We use the term "low-temperature phases" for these materials in reference to the temperature of argon release (as opposed to their formation temperature). Unlike a typical EGA, the released gases were exposed to the Linde 13x zeolite scrubber and an SAES ST175 sintered titanium and molybdenum getter (heated to approximately 300°C) within SAM to purify the noble gases of reactive species (Mahaffy et al., 2012). After the gases were purified, they were first measured by the quadrupole mass spectrometer (QMS) in a low-sensitivity dynamic mode (Farley et al., 2014), similar to a conventional EGA analysis (Sutter et al., 2017) but without the He carrier gas. Upon completion of the dynamic mode measurements, a semistatic mode was initiated wherein a valve pumping the QMS was almost entirely closed to allow a buildup of pressure, increasing sensitivity (Farley et al., 2014). At the end of the semistatic measurement, all gas was pumped out of the manifold while leaving the QMS in scanning mode to enable a determination of the background present in semistatic mode (Vasconcelos et al., 2016). The following sol, an identical procedure was followed with the second heating step, which reached a peak temperature of around 930°C, releasing radiogenic argon from the phases with high release temperatures ("high-temperature phases"). This two-step heating procedure was validated using the SAM testbed instrument on Earth prior to its execution on Mars.

2.5. Quantification of ^{40}Ar

The mass 40 peak in the mass spectrum (M40) is corrected for a small isobaric contribution from the hydrocarbon C_3H_4 using mass 39 (C_3H_3) as a tracer (Figure 2). The ratio of C_3H_4/C_3H_3 was measured to be 0.56 ± 0.02 earlier in the mission during a previous SAM run containing little to no ^{40}Ar. The ^{40}Ar contribution to the mass 40 signal can then be calculated as follows:

$$^{40}\mathrm{Ar} = \mathrm{M40} - \mathrm{M39}\times 0.56. \quad (1)$$

After hydrocarbon isobaric interferences are corrected, the background measured at the end of the run is subtracted from the mass spectrum, yielding what we infer to be the ^{40}Ar peak. In the absence of additional data we cannot correct for Martian atmosphere-derived ^{40}Ar or any other nonradiogenic sources of ^{40}Ar. As previously discussed by Farley et al. (2014), nonradiogenic ^{40}Ar is unlikely to be significant in these ancient K-rich rocks.

3. Results

Here we develop a model for the potassium content of each phase in Mojave 2 and then calculate the K-Ar age of the bulk sample and each step separately using the model. Unless otherwise specified, the word age herein refers to the K-Ar age (i.e., the output of the age equation). Therefore, the terms "bulk age," "model age," "mixed age," and "K-weighted average age" mean the K-Ar age of the entire sample, the K-Ar age of one or more specific components of the sample, the K-Ar age of multiple components of the sample, and the K-Ar age resulting from multiple combined components with differing potassium contents, respectively. The one exception is the phrase "formation age," which refers to the time at which a component physically formed.

3.1. Potassium Partitioning

A model of the K_2O content of each phase in Mojave 2 is vital for assigning ages to the diagenetic and detrital components based on ^{40}Ar release from the low- and high-temperature steps. This problem may be modeled by a simple mass-balance equation:

$$K_T = K_2 + K_1 = K_{plag} + K_{K-spar}{}^{*} + K_{jar} + K_{phyllo} + K_{amorph} \quad (2)$$

$$K_2 = K_{plag} + K_{K-spar}{}^{*} \quad (3)$$

$$K_1 = K_{jar} + K_{phyllo} + K_{amorph} \text{ or } K_1 = K_T - K_2, \quad (4)$$

where K_T is the total potassium in the sample, K_2 and K_1 are the total potassium contents of the phases releasing argon in high-temperature (step 2) and low-temperature (step 1) steps, and K_{plag}, $K_{K\text{-}spar}$*, K_{jar}, K_{phyllo}, and K_{amorph} are the potassium contents of each individual component (plag = plagioclase, K-spar* = potassium feldspar, jar = jarosite, phyllo = phyllosilicate, and amorph = amorphous) weighted by their abundances as determined by CheMin (Table 1). $K_{K\text{-}spar}$* is noted with an asterisk because although potassium feldspar was not detected in the Mojave 2 sample, it has been detected in 8 of the 11 samples drilled thus far in the mission, and thus, we cannot, a priori, rule out the presence of potassium feldspar in Mojave 2 at concentrations below the CheMin detection limit (~1 wt %; Vaniman et al., 2014). The effect that <1 wt % potassium feldspar might have on the step 1 and step 2 model ages is included in the discussion below. The two forms of equation (4) reflect that K_{phyllo} + K_{amorph} are not well constrained by CheMin and thus K_1 is better estimated by difference. Given the bulk K_2O content of the sample and the total amount of ^{40}Ar released during heating ($^{40}Ar_T$), the bulk K-Ar age of the sample is calculated from the ratio:

$$^{40}\mathrm{Ar}_T/K_T. \quad (5)$$

Since the total ^{40}Ar release is simply the sum of ^{40}Ar released in each heating step:

$$^{40}\mathrm{Ar}_T = {}^{40}\mathrm{Ar}_1 + {}^{40}\mathrm{Ar}_2 \quad (6)$$

the model age associated with each step is calculated by

$$^{40}\mathrm{Ar}_2/K_2 \quad (\text{high-T step}) \quad (7)$$

and

$$^{40}\mathrm{Ar}_1/K_1 \text{ or alternatively} {}^{40}\mathrm{Ar}_1/(K_T - K_2) \quad (\text{low-T step}), \quad (8)$$

which is then used to solve the K-Ar age equation, after converting K to ^{40}K:

$$t = \frac{1}{\lambda}\ln\left[\frac{^{40}\mathrm{Ar}}{^{40}\mathrm{K}}\left(\frac{\lambda}{\lambda_e}\right) + 1\right] \quad (9)$$

where t is time since formation, λ is the ^{40}K decay constant ($5.5492 \pm 0.0093 \times 10^{-10}$ a^{-1}; Renne et al., 2010),

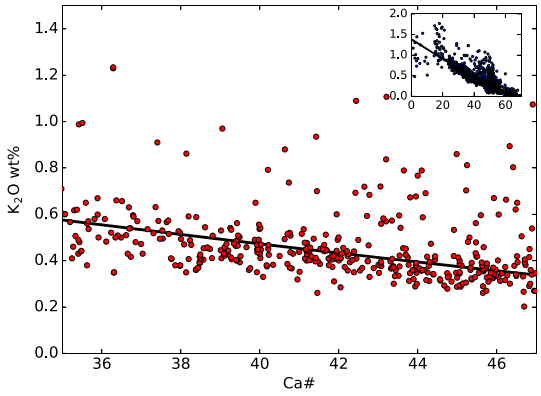

Figure 3. Ca# (or An# as defined in Rampe et al., 2017) versus K_2O content for Martian meteorite plagioclase microprobe analyses (i.e., analyses with molar Or <10%). For the main panel, the data shown are restricted to plagioclase analyses with Ca#s in the range given by Rampe et al. (2017). The inset shows all plagioclase measurements.

and λ_e is the electron capture decay constant ($5.755 \pm 0.016 \times 10^{-11}$ a^{-1}; Renne et al., 2010). It is apparent from equations (7) and (8) that estimating the fraction of the bulk K_2O content measured by APXS that is contained in phases that degas in each of the steps is critical to determining the model step ages and that assumptions made about the potassium contents of these phases will affect the model ages of both steps.

The K_2O content of the plagioclase cannot be directly measured by any instrument onboard Curiosity, but it can be estimated from published analyses of plagioclase in Martian meteorites. The average anorthite content (An, defined as 100 × Ca/(Ca + Na), molar) of Mojave 2 was calculated using plagioclase unit cell parameters that are based on a Rietveld refinement; the resulting value is $An_{41 \pm 6}$ (Rampe et al., 2017). The calculated plagioclase composition for Mojave 2 reported more recently by Morrison et al. (2017) is identical: An_{41}. In both terrestrial plagioclases (e.g., Deer et al., 1997) and Martian meteorite "plagioclases" (e.g., Papike et al., 2009), there is a broad inverse correlation between Ca# (100 × Ca/(Ca + Na), molar) and the K_2O content of the plagioclase, that is, more Na-rich plagioclases have higher K_2O contents. Note that An number mentioned above is equivalent to Ca# and the vast majority of Martian plagioclases are actually maskelynite (e.g., McSween & Treiman, 1998). Based on 1,442 plagioclase analyses from Martian meteorites with 100 × K/(Ca + Na + K) < 10 (molar; a commonly used dividing line between plagioclase and alkali feldspar; Deer et al., 1997), we fit a third-order polynomial to the K_2O content (in weight percent) as a function of Ca# (Figure 3). Fitting was done by minimizing the sum of absolute deviations and all plotted plagioclase compositions satisfy the stoichiometric constraints discussed in Papike et al. (2009). Our data set includes analyses from both the polymict breccia NWA 7034/7533/7475 (of Noachian age; Humayun et al., 2013) and SNCs (plus the orthopyroxenite ALH 84001). All together, these samples span nearly the entire geologic history of Mars and, more importantly, calculated K_2O contents at An_{41} based on fits using just the polymict breccia data or the SNC plus orthopyroxenite data overlap at 1σ. Given the functional relationship shown in Figure 3, the average An content of Mojave 2 translates into a K_2O content of 0.45 ± 0.11 wt % (see section 3.3 for a discussion of uncertainty estimations). Based on this estimate, plagioclase contains around 15% of the total K_2O in Mojave 2, implying that K_{plag} (equations (2) and (3)) is 0.11 ± 0.02 wt % K_2O.

Jarosite forms a solid-solution series with natrojarosite [$NaFe_3(SO_4)_2(OH)$] in nature (e.g., Brophy & Sheridan, 1965; Dutrizac, 1983, 2008), so K_{jar} will vary depending on the amount of sodium that has substituted for potassium in the jarosite structure. The formation of synthetic jarosite with K/(K + Na) < 0.5 requires that the K/(K + Na) of the precipitating solution be <0.1 (Brophy & Sheridan, 1965; Dutrizac, 1983), suggesting that natural jarosites should generally be relatively K rich; this preference is also observed in analyses of natural samples (Dutrizac, 2008). This preference for K over Na is enhanced at low temperatures (Brophy & Sheridan, 1965), and such low temperatures are believed to have been prevalent throughout Gale Crater's history (Vaniman et al., 2014). Based on these considerations of jarosite geochemistry and because the Murray formation does not show strong sodium enrichments (Siebach et al., 2017), we assume limits between pure K endmember and 1:1 K:Na jarosite. As jarosite makes up 3.1 wt % of Mojave 2, this range in K content implies that 40–20% of the potassium in the sample is carried by jarosite, placing K_{jar} in the range 0.29 ± 0.10 to 0.15 ± 0.05 wt % K_2O.

The remaining 45–65% of the K_2O in Mojave 2 must reside in the amorphous and/or phyllosilicate fractions. Amorphous material is common in samples at Gale Crater and has also been measured elsewhere on Mars, by both landed missions and orbiters (Bish et al., 2013; Blake et al., 2013; Morris et al., 2000; Singer, 1985; Vaniman et al., 2014). The likely components of the amorphous phases in Gale Crater, deduced by examining the differences between expected chemistry based on CheMin results and the APXS measurements, include volcanic or impact glass, hisingerite, amorphous sulfate salts, and nanophase iron oxides (Dehouck et al., 2014). Of these phases, the glasses and sulfates are possible hosts of potassium. Below, we examine the likelihood that potassium is held in glass, salts, or phyllosilicates. Determination of which phase(s) contain

potassium is central to the geologic interpretation of the K-Ar age measured. For example, salts, being authigenic and releasing argon at low temperatures, might yield information about when liquid water was most recently present in Gale Crater, while a glass, of either igneous or impact origin, would release argon at high temperature and reflect information about the detrital grains in the sample.

3.1.1. Glass

Putative glass has been observed on Mars from orbit and in aeolian deposits in Gale Crater (Cannon & Mustard, 2015; Minitti et al., 2013), though not in the Gale Crater bedrock. The K_2O contents of Martian glasses can potentially vary from values $<$0.5 wt %, assuming that glasses exist that have bulk compositions similar to those of basaltic shergottites (Treiman & Filiberto, 2015) or the basaltic clasts in NWA 7533 (Humayun et al., 2013) to ~7 wt % if the glasses are either similar in composition to the most silica-rich breccia clast in NWA 7533 or to the compositions of some melt inclusions in Nakhla (e.g., Lee & Chatzitheodoridis, 2016). Given this large range in potassium concentrations, all of the K_2O in the amorphous fraction could hypothetically be accommodated by the presence of a glass with ~2 wt % K_2O (assuming half of the total amorphous content of the sample is glass). However, glass devitrifies to plagioclase and other minerals or dissolves rapidly under most geologic conditions, especially in the presence of water, and even more so in high-ionic strength water (Lofgren, 1970; Wolff-Boenisch et al., 2004). For example, a 1 mm basaltic glass sphere at 25°C will survive only 500 years in moderately acidic conditions (~4,000 years for a glass of rhyolitic composition; Wolff-Boenisch et al., 2004). The Mojave 2 sample, the Pahrump Hills area, and Gale Crater more broadly exhibit abundant evidence for the presence of liquid water at the time of deposition, postdeposition, and during diagenesis (e.g., Gellert et al., 2015; Grotzinger et al., 2014; Nachon et al., 2014; Schieber et al., 2015; Stack et al., 2014). Additionally, modeling efforts suggest that any glass present at the Yellowknife Bay locality has dissolved preferentially (Bridges et al., 2015). We therefore find it unlikely that Mojave 2 contains significant amounts of K_2O in glass.

3.1.2. Salts

Mojave 2 contains 6.19 wt % SO_3, of which only ~1 wt % is held in jarosite, indicating that ~5 wt % SO_3 in Mojave 2 is held in the amorphous phases. Alternatively, the remaining unassigned SO_3 could be present in individual phases at abundances below the ~1 wt % CheMin detection limit, though the lack of any observed evaporites throughout the mission and the large amount of SO_3 that would need to be contained in these minor mineral phases make this possibility unlikely. Additionally, though no Cl-bearing species are present in the crystalline fraction, Mojave 2 contains 0.42 wt % Cl (Rampe et al., 2017). Fluorapatite is present at 1.8 wt % and could host some chlorine, though even if it is pure chlorapatite, it would carry only 0.12 wt % Cl. This relatively high concentration of anions that cannot be linked (via the CheMin analysis; Table 1) to specific minerals containing structural sulfur or chlorine argues for the presence of X-ray amorphous salts in Mojave 2. X-ray amorphous K-bearing sulfate salts have been shown to precipitate from acid sulfate analog brines by cryoprecipitation (Morris et al., 2015). Such amorphous salts are the most likely carriers of a large fraction of the S and Cl in Mojave 2. As potassium is a common cation in salts, X-ray amorphous salts are also likely hosts of potassium in Mojave 2.

3.1.3. Phyllosilicates

Potassium in Mojave 2 could also be held in the phyllosilicate fraction, though the exact amount of K-bearing phyllosilicates in Mojave 2 is difficult to constrain. Illite is the most common phyllosilicate containing potassium. Although K-bearing smectite has been observed terrestrially, these occurrences are rare and require formation conditions not thought to have been present in Gale Crater (e.g., Bischoff, 1972; Dekov et al., 2007). Due to the combination of the relatively subtle peak position shifts between differing phyllosilicate species and the broadness of those peaks, their characterization is difficult using the X-ray diffraction (XRD) pattern generated by the CheMin instrument (Vaniman et al., 2014). However, the 001 spacing of phyllosilicates, a feature that distinguishes illites from smectites, can be deduced from CheMin data (Bristow et al., 2015). The dehydrating conditions within the measurement chamber can cause smectite to collapse, reducing its 001 spacing to approximately that of illite, making the two phases nearly indistinguishable with respect to CheMin (e.g., Bristow et al., 2015; Treiman et al., 2016; Vaniman et al., 2014). Optimization of the Mojave 2 XRD pattern fit suggests that if illite is present, it does not make up a significant portion of the phyllosilicates (T. Bristow, personal communication, 2017). If nanocrystalline or disordered illitic clays are present, they would not appear as distinct peaks but would contribute to the broad "hump" in the XRD pattern that is associated with the amorphous component and thus would be included with that component.

The water peak attributed to dehydroxylation in the SAM EGA can also provide partial constraints on the nature of the phyllosilicate phases in Mojave 2. There are two dehydroxylation peaks in the Mojave 2 EGA pattern. One occurs at >800°C and is more consistent with smectite clay minerals (e.g., saponite) than illite (McAdam et al., 2017). The amount of water released at this high temperature and measured by the SAM EGA is consistent with the weight percent of phyllosilicates calculated from the XRD pattern if the clay minerals are entirely smectite (McAdam et al., 2017). The other dehydroxylation peak occurs at a lower temperature of ~450°C, is attributed to jarosite, and the water abundance is within error of the expected amount based on the CheMin estimate of the mass fraction of jarosite in Mojave 2 (McAdam et al., 2017).

Overall, there are no data precluding K-bearing phyllosilicates in Mojave 2, but nor is there any evidence to support their presence, especially at a high abundance. The exact distribution of K_2O between putative K-phyllosilicate and salt components is unknown and cannot be quantitatively constrained based on the available data, but it appears likely that most or all of the K_2O associated with the low-temperature release of argon not attributable to jarosite is held in X-ray amorphous salt species.

3.2. ^{40}Ar Results

Table 3 shows the ^{40}Ar results obtained from the two heating steps of Mojave 2 (aliquot 2, see paragraph below). In the first step, 3,590 ± 480 pmol/g of ^{40}Ar were measured, while 2,330 ± 320 pmol were measured in the second step. For both steps the hydrocarbon correction was small, ~10% of the mass 40 signal on step 1 and ~5% on step 2. The corrections associated with background measured at the end of the runs was similarly small, a 5% correction to step 1 and a 3% correction to step 2. These corrections are slightly higher than those applied to the Cumberland (Farley et al., 2014) and Windjana (Vasconcelos et al., 2016) samples, mainly because the ^{40}Ar yields were lower during the two individual Mojave 2 heating steps and the amount of hydrocarbons measured in the SAM instrument was somewhat higher.

An initial attempt at noble gas analysis on Mojave 2 ("aliquot 1") was not successfully completed. Upon inlet of the gas released during the first heating step into the quadrupole mass spectrometer during the high-sensitivity semistatic mode, an overpressure condition was generated that caused the experiment to be aborted and the gas to be vented (i.e., the run terminated at the start of the semistatic analysis). Therefore, data were only collected during the low-sensitivity portion of the run. This overpressure condition was possibly due to a buildup of organics in SAM, which had not been fully released during the boil-off stage. The second heating step was conducted as planned. Unexpectedly, the ^{40}Ar yield from step 2 of aliquot 1 (1,640 ± 220 pmol) was ~30% lower than the same step from aliquot 2 (2,330 ± 320 pmol). Using the available low-sensitivity portion of the high-temperature step of aliquot 1, we find that it too was ~30% lower than that measured in aliquot 2. This proportional decrease in ^{40}Ar retrieved from aliquot 1 relative to aliquot 2 is most readily attributed to incomplete sample delivery of aliquot 1, possibly due to loss via a wind gust as the sample was transferred from CHIMRA into SAM.

3.3. Age Calculations and Uncertainties

Combining the total ^{40}Ar release from Mojave 2 (aliquot 2; Table 3) with the APXS K_2O measurement and the modeled sample mass, a bulk K-Ar age of 2.57 ± 0.39 Ga is obtained using equations (6) and (9). Based on the potassium-partitioning model, the ^{40}Ar in step 2 is associated with potassium in detrital feldspar and yields a model age of 4.07 ± 0.63 Ga via equations (7) and (9). The jarosite, phyllosilicates, and/or salts in step 1 combined with the potassium partitioning model indicate a model age of 2.12 ± 0.36 Ga from equations (8) and (9).

Several individual sources of error were combined to quantify the uncertainties on the reported K-Ar ages including the sample mass transfer model (Farley et al., 2014), the APXS measurement of the bulk potassium in the sample, the SAM measurement of ^{40}Ar, and, for the model ages, the mineralogy as measured by CheMin, and the estimates of the potassium contents of the minerals within Mojave 2. The reported uncertainties do not include any potential systematic errors, which cannot be quantified. All uncertainties are reported here at the 1σ uncertainty level. The uncertainty associated with sample delivery is derived from modeling efforts performed at JPL (Farley et al., 2014) and has a relative uncertainty of approximately 13%. The bulk potassium content has an accuracy of 15% of the measured value (R. Gellert, personal communication, 2017). Except where noted, uncertainties associated with the CheMin estimates of the weight fractions

Table 3
Noble Gas Results From Mojave 2

	K_2O (wt %)	^{40}Ar (pmol/g)	K-Ar age (Ga)
Bulk (aliquot 2)	$K_T = 0.73 \pm 0.11$	5920 ± 800	2.57 ± 0.40
Low-temperature step (aliquot 2)	$K_1 = 0.62 \pm 0.11$ (model)	3590 ± 480	2.12 ± 0.36 (model)
High-temperature step (aliquot 2)	$K_2 = 0.11 \pm 0.02$ (model)	2330 ± 320	4.07 ± 0.63[b] (model)
High-temperature step (aliquot 1)[a]	$K_2 = 0.11 \pm 0.02$ (model)	1640 ± 220	3.51 ± 0.61[b] (model)

Note. Uncertainties are reported at the 1σ level.
[a]Data only collected for step 2 of the failed run on aliquot 1. [b]Note that the model ages of the two high-temperature steps are within uncertainty of one another due to uncertainty introduced from the potassium measurement.

of mineral and amorphous phases are taken from the original references (e.g., Rampe et al., 2017; Treiman et al., 2016; Vaniman et al., 2014).

The uncertainty associated with the measurement of ^{40}Ar is calculated for each sweep of the mass spectrum according to the equation:

$$\sigma_{Ar} = \left[\sigma_{40}{}^2 + (K_{HC} \times M39)^2 \times \left((\sigma_{HC}/K_{HC})^2 + (\sigma_{39}/M39)^2\right) + \sigma_{bkgrd}{}^2\right]^{1/2}, \quad (10)$$

where σ indicates the absolute uncertainty of the component in subscript (e.g., σ_{Ar} is the overall ^{40}Ar measurement uncertainty, σ_{HC} is the uncertainty in the hydrocarbon correction, and σ_{bkgrd} is the uncertainty on the background correction). The uncertainty associated with the background correction is taken as the standard error of the mean of the measurements taken after pumpdown (see Figure 2).

The estimated potassium content of the plagioclase in the sample has an uncertainty of 20%, reflecting the stated uncertainty of the An# estimated for the average plagioclase in Mojave 2 by CheMin (Rampe et al., 2017) combined with the standard deviation of the data from the best fit regression line (Figure 3).

The dominant sources of uncertainty in this study are the sample transfer model and the estimates of potassium contents of the various phases. The low abundance of jarosite measured by CheMin has an uncertainty large enough to impact the final age calculations on the model age of the first step.

4. Discussion

Here we discuss the implications of the bulk K-Ar age measured on the Mojave 2 sample, followed by discussion of the model ages for the two temperature steps. We also consider the assumptions regarding the argon retention characteristics of the various phases within the sample and their potential impact on the model ages. Finally, we put these results into the context of the broader geological history of Mars.

4.1. Bulk Age

The bulk age of 2.57 ± 0.39 Ga determined for Mojave 2 is lower than the previous result of 4.21 ± 0.35 Ga from the Cumberland sample (Farley et al., 2014), suggesting that one or more of the potassium-bearing components in Mojave 2 has a formation age younger than the K-Ar age measured at Cumberland. As the sediment source for both samples is thought to be the crater rim and walls (Grotzinger et al., 2015), the detrital plagioclase is unlikely to have a formation age billions of years younger than that measured in Cumberland, implying that the young component in the sample is the jarosite, phyllosilicates, and/or amorphous materials.

4.2. Ages of the Two Steps

4.2.1. High-T Step

The high-temperature step is modeled to record the age of the detrital plagioclase feldspar in Mojave 2. A detrital component model age of 4.07 ± 0.63 Ga is consistent with the previous in situ geochronology experiment at Cumberland (Farley et al., 2014). This model age is sensitive to the mineralogy reported by CheMin, especially whether sanidine was present at low concentrations in the sample. Sanidine was not detected by CheMin in Mojave 2, but many of the rocks analyzed at Gale Crater do carry sanidine (Rampe et al., 2017; Treiman et al., 2016; Vaniman et al., 2014). If sanidine was, in fact, present in Mojave 2 but below the detection limit of CheMin (~1 wt %), its ^{40}Ar would be released either completely or partially during the high-temperature step. By analogy with the Cumberland sample (also a mudstone) that contained

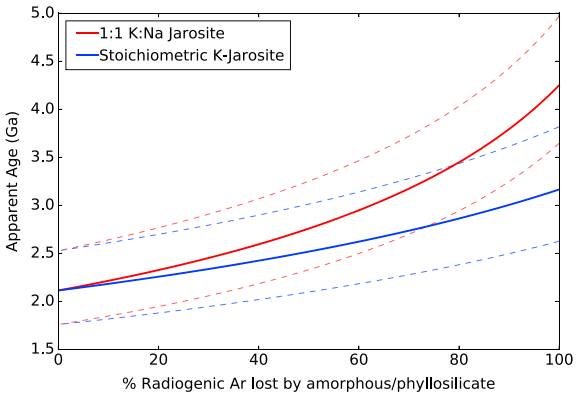

Figure 4. Potential ages of the low-temperature materials given varied argon retention in the amorphous/phyllosilicate fraction. The most likely values are shown with solid lines; 1σ uncertainties are shown with dashed lines. End-member cases of jarosite composition (stoichiometric K jarosite and 1:1 K:Na jarosite) are shown in blue and red, respectively.

1.6 wt % K-feldspar and completely (or almost completely) degassed (Farley et al., 2014), we assume that any sanidine in the Mojave 2 sample would also have degassed thoroughly during the high-temperature step. However, its potassium content would have been incorrectly assigned to the low-temperature step rather than the high-temperature step. This would have implications for the model ages of both steps (equations (7) and (8)), with the age of step 2 needing to be revised downward and the age of step 1 revised upward.

A limit to how large this effect could be is obtained by considering the plausible formation ages of the Gale Crater feldspars. Detrital minerals in Mojave 2 are most likely older than the crater, being sourced from the crater target rocks, making their plausible formation age >3.6 Ga (Le Deit et al., 2012; Thomson et al., 2011). If more than 0.25 wt % end-member sanidine was present in the sample, the model age for step 2 would fall below 3.6 Ga. This is a reasonable upper limit on the amount of undetected sanidine in Mojave 2. By mass balance, the increase in the low-temperature step model age due to <0.25 wt % sanidine is <4% of the age (well within the stated uncertainty). Thus, the step 1 model age is robust to the presence of plausible amounts of sanidine.

4.2.2. Low-T Step

The model age of 2.12 ± 0.36 Ga measured in step 1 is a mixed age involving jarosite and amorphous/phyllosilicate fractions (Table 3). We cannot specifically disentangle the ages of these individual components, resulting in two possibilities: (1) the jarosite and amorphous/phyllosilicate components have the same K-Ar age or (2) the step 1 model age is a mixture of two or more different K-Ar ages. In the first scenario, assuming complete argon retention, the model age of 2.12 ± 0.36 Ga represents the formation age of both of these components and most likely reflects a single fluid flow event, which formed or recrystallized the secondary phases in Mojave 2 at that time, consistent with the interpretations of Rampe et al. (2017). In the second scenario, the step 1 model age is a K-weighted average age of the jarosite and other low-temperature K-bearing components in the sample, meaning at least one phase has a K-Ar age of $\lesssim$2 Ga. The only potential scenario in which both phases have a formation age older than the model age is in the case of argon loss, which is explored in the following section.

4.3. Argon Loss From Phases in the Low-Temperature Step

A K-Ar age is only equivalent to a mineral formation age in the case of a closed system. Thus, we must consider that a potential reason for the observation of a young K-Ar age at Mojave 2 is the loss of radiogenic argon from one or more of the low-temperature phases at any time prior to those phases being analyzed in SAM. This loss could have occurred via solution reprecipitation (i.e., as a result of fluid migration events), by diffusion over geologic time, during sample drilling and handling, or as a result of the brief low-temperature (<150°C) boil-off step applied to the sample to release adsorbed volatiles. If radiogenic ^{40}Ar was lost before being measured by SAM, the K-Ar age of the low-temperature components would be younger than their formation age or ages. Jarosite is known to retain ^{40}Ar over geologic time at temperatures up to ~150°C (Kula & Baldwin, 2011; Vasconcelos et al., 1994). Therefore, if one of the components in Mojave 2 has lost significant argon, it is unlikely to be the jarosite.

We next assess the K-weighted average age of step 1 based on a full range (0–100%) of Ar retention in the low-temperature phases excluding jarosite (Figure 4). If all of these phases are fully retentive with respect to argon, then the K-weighted average formation age of step 1 is 2.12 ± 0.36 Ga, as calculated, suggesting a single age resetting event occurred at this time (see section 4.4 below for discussion of this possibility). If the amorphous/phyllosilicate fraction has lost all of its argon (making that component's K-Ar age zero), the model age of the jarosite alone would be 3.17 ± 0.60 Ga, placing a firm upper limit on its formation age if it were endmember jarosite [i.e., $KFe_3(SO_4)_2(OH)_6$]. Decreasing the K content of the jarosite increases its model age in this scenario. However, as described above, K-rich jarosite is geochemically likely (Dutrizac, 2008). For a reasonable lower compositional limit of 1:1 K:Na, the model age of the jarosite alone is 4.25 ± 0.66 Ga.

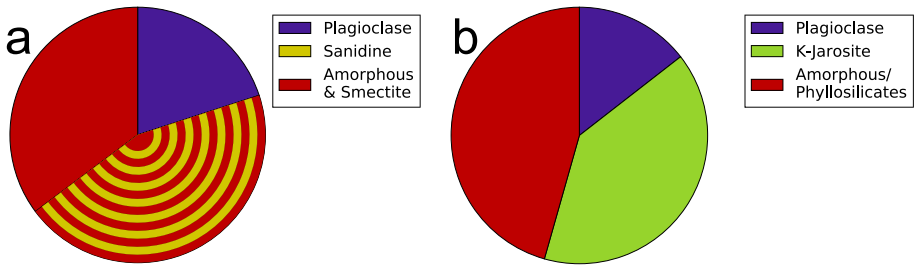

Figure 5. Comparison of the distribution of potassium between minerals in (a) Cumberland and (b) Mojave 2. The sanidine in Cumberland is at the detection limit; stripes indicate that the K_2O held in sanidine will trade off against the amorphous and phyllosilicate fraction depending on the true amount of sanidine in the sample.

Without strong constraints on the actual phases making up the amorphous/phyllosilicate fraction, it is difficult to constrain the extent to which this fraction has lost argon by natural processes. Illite has an argon closure temperature of around 100°C on timescales of millions of years (e.g., Evernden et al., 1960; Hamilton et al., 1989); mineral assemblages present in the drilled Cumberland and John Klein samples suggest burial temperatures <80°C (Vaniman et al., 2014), arguing against potential ^{40}Ar loss from putative illite in Mojave 2. Possible potassium-containing salts in Mojave 2 likely also retain radiogenic argon over geologic time against diffusive loss. Several sulfate and chloride salts have been determined to be useful for Ar dating (e.g., Leitner et al., 2014; Renne et al., 2001; Smits & Gentner, 1950), although there are no data on Ar closure temperatures for these phases. It has been suggested that liquid brines in the near subsurface may occur in Gale Crater from deliquescing of perchlorate in the soil (Martín-Torres et al., 2015). The possibility exists that these brines have reprecipitated salts within Mojave 2, resetting their ages. However, jarosite is dissolved relatively rapidly in the presence of circumneutral water (Madden, Bodnar, & Rimstidt, 2004); jarosite's presence in the sample argues against resetting of any salts in Mojave 2 by the presence of liquid water after their initial deposition. The presence of a brine would be unlikely to affect the argon retention of phyllosilicates.

Crystalline hydrated salts have been observed to lose their water under the extremely dry conditions inside CheMin, causing salts that were crystalline to appear X-ray amorphous (Vaniman et al., 2014). This process could have occurred with K-bearing hydrated salts in Mojave 2. If a similar phenomenon occurs within SAM during sample processing before analysis, most likely as a result of the boil-off stage (150°C maximum), the change in mineral structure could cause the loss of significant amounts of argon from these phases. However, the evolved water trace in the Mojave EGA below 150°C is minimal and mostly attributed to the release of adsorbed water (Sutter et al., 2017), suggesting that argon loss coincident with dehydration during the boil-off stage is unlikely. Phyllosilicate phases would also be unlikely to lose significant amounts of argon at 150°C (Evernden et al., 1960).

The K-Ar geochronology result on the Cumberland sample (Farley et al., 2014) provides additional insight into the issue of Ar retention. Like Mojave 2, the amorphous and/or phyllosilicate components in Cumberland were a significant host of potassium (Figure 5). Cumberland's bulk K-Ar age was measured to be 4.21 ± 0.35 Ga (Farley et al., 2014); if greater than 25% of the argon contained in the amorphous/phyllosilicate fraction was lost prior to analysis, the K-Ar age of the sample corrected for Ar loss would exceed the age of Mars. By analogy between Cumberland and Mojave 2, more than 25% Ar loss in the amorphous and/or phyllosilicate fractions of Mojave 2 seems unlikely. To put this degree of loss in perspective, more than 90% Ar loss from these phases would be required to cause the loss-corrected model age of the low-*T* phases in Mojave 2 to exceed 3.0 Ga (60% if the jarosite in the sample has 1:1 K:Na rather than pure K jarosite). Therefore, it appears that the K-weighted average formation age of the low-*T* components in Mojave 2 is <3.0 Ga, indicating that at least one major phase in Mojave 2 was formed or recrystallized well after the Hesperian period on Mars. Given that the only major mineralogical difference between Cumberland and Mojave 2 is the presence of jarosite, if the jarosite and evaporite/phyllosilicate phases have different formation ages (i.e., Mojave 2 reflects the second scenario described above in section 4.2.2), jarosite appears most likely to be this young component.

4.4. Implications of Young Components in Mojave 2

The most noteworthy result from the low-temperature step is the young model age attributable to the phase or phases in Mojave 2 whose genesis reflects an interaction with water, indicating a likely formation age of

the jarosite and potentially the K-bearing salts and/or phyllosilicates of less than 3 Ga. This young age is potentially an indication of the most recent aqueous activity at Mojave 2. It is possible that this last aqueous activity occurred in the final stages of the drying of the lake in Gale Crater, implying that the lake (and therefore the presence of large perennial bodies of water on Mars) was much longer-lived than previously thought (Bristow et al., 2015; Grotzinger et al., 2015). However, the presence of such a long-lived lake would contravene the generally understood geologic history of water on Mars (Bibring et al., 2006). It is more likely that the formation age (or ages) of these diagenetic materials is related to postdepositional subsurface fluid flow. There are a number of diagenetic features in Mojave 2 and in the surrounding bedrock that are indicative of water/rock interaction and postdepositional fluids (Gellert et al., 2015; Grotzinger et al., 2015; McBride et al., 2015; Nachon et al., 2017; Schieber et al., 2015). We postulate that the crystal laths observed in Mojave 2 (Figure 1; McBride et al., 2015; Schieber et al., 2015) could have been redissolved by such a fluid during precipitation of the jarosite. Specifically, Rampe et al. (2017) suggest that after mudstone deposition in a circumneutral, relatively reducing lake environment, one or more influxes of oxidizing acidic fluids could have produced the jarosite in Mojave 2. Additionally, young alluvial fans and chloride deposits hint at minor fluvial activity extending well into the Amazonian in the vicinity of Gale Crater (Ehlmann & Buz, 2015; Grant et al., 2014). These late fluvial features reinforce the prospect of relatively young water-lain minerals inside Gale Crater.

Evidence of relatively recent water activity in Gale Crater is paralleled by alteration features in the Nakhlite Martian meteorites (Changela & Bridges, 2010; Hicks et al., 2014) that substantially postdate the meteorites' crystallization ages. These alteration features (small veinlets of carbonate, ferric saponite, serpentine, and amorphous gel), historically described as "iddingsite" (see Treiman, 2005, for an overview), have been dated to the Amazonian period with a maximum age of 670 Ma by the K-Ar method (Swindle et al., 2000). This alteration age is much younger than the crystallization age of ~1.3 Ga determined for the nakhlite host rocks (Nyquist et al., 2001) and is attributed to impact-generated hydrothermal activity (Changela & Bridges, 2010; Schwenzer et al., 2012).

Recurring slope lineae are contemporary slope-darkening streaks observed on Mars (e.g., McEwen et al., 2014, 2011). These transient features occur on Sun-facing slopes during the warmest period of the year and are suggested to be associated with hydrated salts such as perchlorates (Ojha et al., 2014, 2015), potentially indicating that they are formed via liquid brine flows. These modern observations, taken in combination with the young alteration features in the nakhlite meteorites and the young K-Ar age observed at Mojave 2 associated with water-lain features, suggest that liquid water at or near the surface of Mars has been at least episodically (though perhaps only locally) available since the Hesperian-Amazonian transition and likely throughout the planet's geologic history.

5. Conclusions

A third radiometric dating experiment has been conducted on Mars using the SAM instrument on the Curiosity rover, yielding a bulk K-Ar age of 2.57 ± 0.39 Ga on the Mojave 2 mudstone. A new two-step heating methodology resulted in separate model ages of what we infer to be detrital feldspar and diagenetic components of the Mojave 2 sample of 4.07 ± 0.63 Ga and 2.12 ± 0.36 Ga, respectively. The ancient age of the detrital component is consistent with previous results and the expected age of igneous material in Gale Crater. The young K-Ar age of the diagenetic component could reflect a formation age or could result from ^{40}Ar loss from the amorphous/phyllosilicate component before measurement, either in nature or in the SAM instrument. Given a full range of argon retention in the amorphous/phyllosilicate component, the model K-weighted average age of the low-temperature phases extends from 2.12 ± 0.36 Ga if argon is quantitatively retained in all phases to a jarosite model age of 3.17 ± 0.60 Ga if argon is completely lost from the amorphous/phyllosilicate portion (4.25 ± 0.66 Ga in the case of more K-poor 1:1 K:Na jarosite). By analysis of the likely sample components and by comparison to Cumberland, the argon loss from the phyllosilicate/amorphous phase(s) appears unlikely to be substantial, making the likely K-weighted average age of the low-temperature materials $<$3.0 Ga, corrected for any minor argon loss. This age indicates that at least one of these components was formed well into the Amazonian, after aqueous activity on Mars is thought to have largely stopped and is inconsistent with precipitation from the desiccation of the lake in Gale Crater. The prevalent diagenetic features in Mojave 2 and the surrounding bedrock suggestive of

postdepositional fluid flow may be associated with this relatively young age, which is potentially indicative of the most recent liquid water activity at the Mojave 2 drill site. In concert with alteration patterns in meteorites and modern observations of liquid surface water, these results suggest that liquid water has potentially been available at or near the surface of Mars throughout its history.

Acknowledgments
We thank George Rossmann, Tom Bristow, Liz Rampe, Dick Morris, and Paul Asimow for numerous helpful discussions. We are indebted to the MSL science and engineering teams, who made (and continue to make) this work possible. Data contained in this paper are publicly available on the Planetary Data System (PDS; pds.nasa.gov). Funding was provided by NASA.

References

Amirkhanoff, K. I., Brandt, S., & Bartnitsky, E. (1961). Radiogenic argon in minerals and its migration. *Annals of the New York Academy of Sciences*, *91*(1), 235–275.

Anderson, R. C., Jandura, L., Okon, A., Sunshine, D., Roumeliotis, C., Beegle, L., … Brown, K. (2012). Collecting samples in Gale Crater, Mars; an overview of the Mars Science Laboratory sample acquisition, sample processing and handling system. *Space Science Reviews*, *170*(1–4), 57–75. https://doi.org/10.1007/s11214-012-9898-9

Bibring, J.-P., Langevin, Y., Mustard, J. F., Poulet, F., Arvidson, R., Gendrin, A., … Neukum, G. (2006). Global mineralogical and aqueous Mars history derived from OMEGA/Mars Express data. *Science*, *312*(5772), 400–404. https://doi.org/10.1126/science.1122659

Bischoff, J. L. (1972). A ferroan nontronite from the Red Sea geothermal system. *Clays and Clay Minerals*, *20*(4), 217–223. https://doi.org/10.1346/CCMN.1972.0200406

Bish, D. L., Blake, D., Vaniman, D., Chipera, S., Morris, R., Ming, D., … Spanovich, N. (2013). X-ray diffraction results from Mars Science Laboratory: Mineralogy of Rocknest at Gale Crater. *Science*, *341*(6153), 1238932. https://doi.org/10.1126/science.1238932

Blake, D. F., Morris, R. V., Kocurek, G., Morrison, S., Downs, R. T., Bish, D., … Sarrazin, P. (2013). Curiosity at Gale Crater, Mars: Characterization and analysis of the Rocknest sand shadow. *Science*, *341*(6153), 1239505. https://doi.org/10.1126/science.1239505

Bogard, D., Husain, L., & Nyquist, L. (1979). ^{40}Ar-^{39}Ar age of the Shergotty achondrite and implications for its post-shock thermal history. *Geochimica et Cosmochimica Acta*, *43*(7), 1047–1055. https://doi.org/10.1016/0016-7037(79)90093-0

Bridges, J. C., Schwenzer, S., Leveille, R., Westall, F., Wiens, R., Mangold, N., … Berger, G. (2015). Diagenesis and clay mineral formation at Gale Crater, Mars. *Journal of Geophysical Research: Planets*, *120*, 1–19. https://doi.org/10.1002/2014JE004757

Bristow, T. F., Bish, D. L., Vaniman, D. T., Morris, R. V., Blake, D. F., Grotzinger, J. P., … McAdam, A. C. (2015). The origin and implications of clay minerals from Yellowknife Bay, Gale Crater, Mars. *American Mineralogist*, *100*(4), 824–836. https://doi.org/10.2138/am-2015-5077CCBYNCND

Brophy, G. P., & Sheridan, M. F. (1965). Sulfate studies IV: The jarosite-natrojarosite-hydronium jarosite solid solution series. *American Mineralogist*, *50*, 1595–1607.

Cannon, K. M., & Mustard, J. F. (2015). Preserved glass-rich impactites on Mars. *Geology*, *43*(7), 635–638. https://doi.org/10.1130/G36953.1

Cassata, W. S., Renne, P. R., & Shuster, D. L. (2009). Argon diffusion in plagioclase and implications for thermochronometry: A case study from the Bushveld Complex, South Africa. *Geochimica et Cosmochimica Acta*, *73*(21), 6600–6612.

Cassata, W. S., Renne, P. R., & Shuster, D. L. (2011). Argon diffusion in pyroxenes: Implications for thermochronometry and mantle degassing. *Earth and Planetary Science Letters*, *304*(3–4), 407–416. https://doi.org/10.1016/j.epsl.2011.02.019

Changela, H., & Bridges, J. (2010). Alteration assemblages in the nakhlites: Variation with depth on Mars. *Meteoritics & Planetary Science*, *45*(12), 1847–1867. https://doi.org/10.1111/j.1945-5100.2010.01123.x

Deer, W. A., Howie, R. A., & Zussman, J. (1997). *Rock-forming minerals: Single-chain silicates* (Vol. 2A). London, UK: Geological Society of London.

Dehouck, E., McLennan, S. M., Meslin, P. Y., & Cousin, A. (2014). Constraints on abundance, composition, and nature of X-ray amorphous components of soils and rocks at Gale Crater, Mars. *Journal of Geophysical Research: Planets*, *119*, 2640–2657. https://doi.org/10.1002/2014JE004716

Dekov, V. M., Kamenov, G. D., Stummeyer, J., Thiry, M., Savelli, C., Shanks, W. C., … Vértes, A. (2007). Hydrothermal nontronite formation at Eolo Seamount (Aeolian volcanic arc, Tyrrhenian Sea). *Chemical Geology*, *245*(1–2), 103–119. https://doi.org/10.1016/j.chemgeo.2007.08.006

Dutrizac, J. (1983). Factors affecting alkali jarosite precipitation. *Metallurgical Transactions B*, *14*(4), 531–539. https://doi.org/10.1007/BF02653939

Dutrizac, J. (2008). Factors affecting the precipitation of potassium jarosite in sulfate and chloride media. *Metallurgical and Materials Transactions B*, *39*(6), 771–783. https://doi.org/10.1007/s11663-008-9198-7

Ehlmann, B. L., & Buz, J. (2015). Mineralogy and fluvial history of the watersheds of Gale, Knobel, and Sharp craters: A regional context for the Mars Science Laboratory Curiosity's exploration. *Geophysical Research Letters*, *42*(2), 264–273. https://doi.org/10.1002/2014GL062553

Ehlmann, B. L., Mustard, J. F., Murchie, S. L., Bibring, J.-P., Meunier, A., Fraeman, A. A., & Langevin, Y. (2011). Subsurface water and clay mineral formation during the early history of Mars. *Nature*, *479*(7371), 53–60. https://doi.org/10.1038/nature10582

Evernden, J. F., Curtis, G. H., Kistler, R., & Obradovich, J. (1960). Argon diffusion in glauconite, microcline, sanidine, leucite and phlogopite. *American Journal of Science*, *258*(8), 583–604. https://doi.org/10.2475/ajs.258.8.583

Farley, K., Malespin, C., Mahaffy, P., Grotzinger, J., Vasconcelos, P., Milliken, R., … Wimmer-Schweingruber, R. (2014). In situ radiometric and exposure age dating of the Martian surface. *Science*, *343*(6169), 1247166. https://doi.org/10.1126/science.1247166

Fassett, C. I., & Head, J. W. (2008). The timing of Martian valley network activity: Constraints from buffered crater counting. *Icarus*, *195*(1), 61–89. https://doi.org/10.1016/j.icarus.2007.12.009

Freissinet, C., Glavin, D., Mahaffy, P. R., Miller, K., Eigenbrode, J., Summons, R., … Zorzano, M.-P. (2015). Organic molecules in the sheepbed mudstone, Gale Crater, mars. *Journal of Geophysical Research: Planets*, *120*, 495–514. https://doi.org/10.1002/2014JE004737

Gellert, R., Berger, J., Boyd, N., Campbell, J., Desouza, E., Elliott, B., … Yen, A. (2015). Chemical evidence for an aqueous history at Pahrump, Gale Crater, Mars, as seen by the APXS, *Lunar and Planetary Science Conference*, Abstract 1855.

Glavin, D. P., Freissinet, C., Miller, K. E., Eigenbrode, J. L., Brunner, A. E., Buch, A., … Mahaffy, P. R. (2013). Evidence for perchlorates and the origin of chlorinated hydrocarbons detected by SAM at the Rocknest aeolian deposit in Gale Crater. *Journal of Geophysical Research: Planets*, *118*, 1955–1973. https://doi.org/ 10.1002/jgre.20144

Gombosi, D. J., Baldwin, S. L., Watson, E. B., Swindle, T. D., Delano, J. W., & Roberge, W. G. (2015). Argon diffusion in Apollo 16 impact glass spherules: Implications for ^{40}Ar/^{39}Ar dating of lunar impact events. *Geochimica et Cosmochimica Acta*, *148*, 251–268. https://doi.org/10.1016/j.gca.2014.09.031

Grant, J. A., Wilson, S. A., Mangold, N., Calef, F., & Grotzinger, J. P. (2014). The timing of alluvial activity in Gale Crater, Mars. *Geophysical Research Letters*, *41*(4), 1142–1149. https://doi.org/10.1002/2013GL058909

Grotzinger, J. P., Sumner, D. Y., Kah, L., Stack, K., Gupta, S., Edgar, L., … Yingst, A. (2014). A habitable fluvio-lacustrine environment at Yellowknife Bay, Gale Crater, Mars. *Science*, *343*(6169), 1242777. https://doi.org/10.1126/science.1242777

Grotzinger, J., Gupta, S., Malin, M., Rubin, D., Schieber, J., Siebach, K., … Wilson, S. (2015). Deposition, exhumation, and paleoclimate of an ancient lake deposit, Gale Crater, Mars. *Science*, *350*(6257), aac7575. https://doi.org/10.1126/science.aac7575

Halliday, A. (1978). ^{40}Ar-^{39}Ar stepheating studies of clay concentrates from Irish orebodies. *Geochimica et Cosmochimica Acta*, *42*(12), 1851–1858. https://doi.org/10.1016/0016-7037(78)90240-5

Hamilton, P., Kelley, S., & Fallick, A. E. (1989). K-Ar dating of illite in hydrocarbon reservoirs. *Clay Minerals*, *24*(2), 215–231. https://doi.org/10.1180/claymin.1989.024.2.08

Hartmann, W. K. (2005). Martian cratering 8: Isochron refinement and the chronology of Mars. *Icarus*, *174*(2), 294–320. https://doi.org/10.1016/j.icarus.2004.11.023

Hartmann, W., & Daubar, I. (2017). Martian cratering 11. Utilizing decameter scale crater populations to study Martian history. *Meteoritics & Planetary Science*, *52*(3), 493–510. https://doi.org/10.1111/maps.12807

Hartmann, W. K., & Neukum, G. (2001). Cratering chronology and the evolution of Mars. *Space Science Reviews*, *96*(1–4), 165–194. https://doi.org/10.1023/A:1011945222010

Hassanipak, A., & Wampler, J. (1996). Radiogenic argon released by stepwise heating of glauconite and illite: The influence of composition and particle size. *Clays and Clay Minerals*, *44*(6), 717–726. https://doi.org/10.1346/CCMN.1996.0440601

Hicks, L. J., Bridges, J. C., & Gurman, S. (2014). Ferric saponite and serpentine in the nakhlite Martian meteorites. *Geochimica et Cosmochimica Acta*, *136*, 194–210. https://doi.org/10.1016/j.gca.2014.04.010

Humayun, M., Nemchin, A., Zanda, B., Hewins, R., Grange, M., Kennedy, A., … Deldicque, D. (2013). Origin and age of the earliest Martian crust from meteorite NWA7533. *Nature*, *503*(7477), 513–516. https://doi.org/10.1038/nature12764

Kula, J., & Baldwin, S. L. (2011). Jarosite, argon diffusion, and dating aqueous mineralization on earth and Mars. *Earth and Planetary Science Letters*, *310*(3–4), 314–318. https://doi.org/10.1016/j.epsl.2011.08.006

Le Deit, L., Hauber, E., Fueten, F., Mangold, N., Pondrelli, M., Rossi, A., & Jaumann, R. (2012). Model age of Gale Crater and origin of its layered deposits. *Third Conference on Early Mars.*, Abstract 7045.

Lee, M. R., & Chatzitheodoridis, E. (2016). Replacement of glass in the Nakhla meteorite by berthierine: Implications for understanding the origins of aluminum-rich phyllosilicates on Mars. *Meteoritics & Planetary Science*, *51*(9), 1643–1653. https://doi.org/10.1111/maps.12687

Leitner, C., Neubauer, F., Genser, J., Borojević-Šoštarić, S., & Rantitsch, G. (2014). ^{40}Ar/^{39}Ar ages of crystallization and recrystallization of rock-forming polyhalite in Alpine rocksalt deposits. *Geological Society, London, Special Publications*, *378*, 207–224. https://doi.org/10.1144/SP378.5

Lofgren, G. (1970). Experimental devitrification rate of rhyolite glass. *Geological Society of America Bulletin*, *81*(2), 553–560.

Madden, M. E., Bodnar, R., & Rimstidt, J. (2004). Jarosite as an indicator of water-limited chemical weathering on Mars. *Nature*, *431*(7010), 821–823. https://doi.org/10.1038/nature02971

Mahaffy, P. R., Webster, C. R., Cabane, M., Conrad, P. G., Coll, P., Atreya, S. K., … Mumm, E. (2012). The sample analysis at Mars investigation and instrument suite. *Space Science Reviews*, *170*(1–4), 401–478. https://doi.org/10.1007/s11214-012-9879-z

Martín-Torres, F. J., Zorzano, M.-P., Valentín-Serrano, P., Harri, A.-M., Genzer, M., Kemppinen, O., … Vaniman, D. (2015). Transient liquid water and water activity at Gale Crater on Mars. *Nature Geoscience*, *8*(5), 357–361. https://doi.org/10.1038/ngeo2412

McAdam, A., Sutter, B., Franz, H., Hogancamp, J., Knudson, C., Andrejkovicova, S., … Mahaffy, P. (2017). Constraints on the mineralogy of Gale Crater mudstones from MSL SAM evolved water, *Lunar and Planetary Sciences Conference*, Abstract 1853.

McBride, M., Manitti, M., Stack, K., Yingst, R., Edgett, K., Goetz, W., … Van Beek, J. (2015). Mars Hand Lens Imager (MAHLI) observations at the Pahrump Hills field site, Gale Crater, *Lunar and Planetary Science Conference*, Abstract 2855.

McEwen, A. S., Preblich, B. S., Turtle, E. P., Artemieva, N. A., Golombek, M. P., Hurst, M., … Christensen, P. R. (2005). The rayed crater Zunil and interpretations of small impact craters on Mars. *Icarus*, *176*(2), 351–381. https://doi.org/10.1016/j.icarus.2005.02.009

McEwen, A. S., Ojha, L., Dundas, C. M., Mattson, S. S., Byrne, S., Wray, J. J., … Gulick, V. C. (2011). Seasonal flows on warm Martian slopes. *Science*, *333*(6043), 740–743. https://doi.org/10.1126/science.1204816

McEwen, A. S., Dundas, C. M., Mattson, S. S., Toigo, A. D., Ojha, L., Wray, J. J., … Thomas, N. (2014). Recurring slope lineae in equatorial regions of Mars. *Nature Geoscience*, *7*(1), 53–58.

McSween, H. Y., & Treiman, A. H. (1998). Martian meteorites. *Reviews in Mineralogy and Geochemistry*, *36*(1), 6.1–6.53.

Mees, F., Casteñeda, C., Herrero, J., & Van Ranst, E. (2012). The nature and significance of variations in gypsum crystal morphology in dry lake basins. *Journal of Sedimentary Research*, *82*(1), 37–52.

Ming, D., Archer, P., Glavin, D., Eigenbrode, J., Franz, H., Sutter, B., … Yingst, A. (2014). Volatile and organic compositions of sedimentary rocks in Yellowknife Bay, Gale Crater, Mars. *Science*, *343*(6169), 1245267. https://doi.org/10.1126/science.1245267

Minitti, M., Kah, L., Yingst, R., Edgett, K., Anderson, R., Beegle, L., … Van Beek, T. (2013). MAHLI at the Rocknest sand shadow: Science and science-enabling activities. *Journal of Geophysical Research: Planets*, *118*, 2338–2360. https://doi.org/10.1002/2013JE004426

Morris, R. V., Golden, D., Bell, J. F., Shelfer, T. D., Scheinost, A. C., Hinman, N. W., … Britt, D. T. (2000). Mineralogy, composition, and alteration of Mars Pathfinder rocks and soils: Evidence from multispectral, elemental, and magnetic data on terrestrial analogue, SNC meteorite, and Pathfinder samples. *Journal of Geophysical Research*, *105*(E1), 1757–1817. https://doi.org/10.1029/1999JE001059

Morris, R., Rampe, E., Graff, T., Archer, P. Jr, Le, L., Ming, D., & Sutter, B. (2015). Transmission X-ray diffraction (XRD) patterns relevant to the MSL CheMin amorphous component: Sulfates and silicates, *Lunar and Planetart Sciences Conference*, Abstract 2434.

Morrison, S. M., Downs, R. T., Blake, D. F., Vaniman, D. T., Ming, D. W., Hazen, R. M., … Craig, P. I. (2017). Crystal chemistry of Martian minerals from Bradbury Landing through Naukluft Plateau, Gale Crater, Mars. *American Mineralogist*. https://doi.org/10.2138/am-2018-6123

Nachon, M., Clegg, S., Mangold, N., Schröder, S., Kah, L., Dromart, G., … Wellington, D. (2014). Calcium sulfate veins characterized by ChemCam/Curiosity at Gale Crater, Mars. *Journal of Geophysical Research: Planets*, *119*, 1991–2016. https://doi.org/10.1002/2013JE004588

Nachon, M., Mangold, N., Forni, O., Kah, L. C., Cousin, A., Wiens, R. C., … Sumner, D. (2017). Chemistry of diagenetic features analyzed by ChemCam at Pahrump Hills, Gale Crater, Mars. *Icarus*, *281*, 121–136. https://doi.org/10.1016/j.icarus.2016.08.026

Nimmo, F., & Tanaka, K. (2005). Early crustal evolution of Mars. *Annual Review of Earth and Planetary Sciences*, *33*, 133–161.

Nyquist, L., Bogard, D., Shih, C.-Y., Greshake, A., Stöffler, D., & Eugster, O. (2001). Ages and geologic histories of Martian meteorites. *Space Science Reviews*, *96*(12), 105–164. https://doi.org/10.1023/A:1011993105172

Ojha, L., McEwen, A., Dundas, C., Byrne, S., Mattson, S., Wray, J., … Schaefer, E. (2014). HiRISE observations of recurring slope lineae (RSL) during southern summer on Mars. *Icarus*, *231*, 365–376.

Ojha, L., Wilhelm, M. B., Murchie, S. L., McEwen, A. S., Wray, J. J., Hanley, J., … Chojnacki, M. (2015). Spectral evidence for hydrated salts in recurring slope lineae on Mars. *Nature Geoscience*, *8*(11), 829–832. https://doi.org/10.1038/ngeo2546

Papike, J., Karner, J., Shearer, C., & Burger, P. (2009). Silicate mineralogy of Martian meteorites. *Geochimica et Cosmochimica Acta*, *73*(24), 7443–7485. https://doi.org/10.1016/j.gca.2009.09.008

Rampe, E., Ming, D., Blake, D., Bristow, T., Chipera, S., Grotzinger, J., … Ach, C. (2017). Mineralogy of an ancient lacustrine mudstone succession from the Murray formation, Gale Crater, Mars. *Earth and Planetary Science Letters*, *471*, 172–185. https://doi.org/10.1016/j.epsl.2017.04.021

Renne, P. R., Sharp, W. D., Montañez, I. P., Becker, T. A., & Zierenberg, R. A. (2001). $^{40}Ar/^{39}Ar$ dating of Late Permian evaporites, southeastern New Mexico, USA. *Earth and Planetary Science Letters*, *193*(3–4), 539–547. https://doi.org/10.1016/S0012-821X(01)00525-8

Renne, P. R., Mundil, R., Balco, G., Min, K., & Ludwig, K. R. (2010). Joint determination of ^{40}K decay constants and $^{40}Ar^*/^{40}K$ for the Fish Canyon sanidine standard, and improved accuracy for $^{40}Ar/^{39}Ar$ geochronology. *Geochimica et Cosmochimica Acta*, *74*(18), 5349–5367. https://doi.org/10.1016/j.gca.2010.06.017

Robbins, S. J., Antonenko, I., Kirchoff, M. R., Chapman, C. R., Fassett, C. I., Herrick, R. R., … Huang, D. (2014). The variability of crater identification among expert and community crater analysts. *Icarus*, *234*, 109–131. https://doi.org/10.1016/j.icarus.2014.02.022

Schieber, J., Sumner, D., Bish, D., Stack, K., Minitti, M., Yingst, A., … Grotzinger, J. (2015). The Pahrump succession in Gale Crater—A potential evaporite bearing lacustrine mudstone with resemblance to Earth analogs, *Lunar and Planetary Science Conference*, Abstract 2153.

Schwenzer, S., Abramov, O., Allen, C., Clifford, S., Cockell, C., Filiberto, J., … Wiens, R. (2012). Puncturing Mars: How impact craters interact with the Martian cryosphere. *Earth and Planetary Science Letters*, *335–336*, 9–17.

Siebach, K., Baker, M., Grotzinger, J., McLennan, S., Gellert, R., Thompson, L., & Hurowitz, J. (2017). Sorting out compositional trends in sedimentary rocks of the Bradbury group (Aeolis Palus), Gale Crater, Mars. *Journal of Geophysical Research: Planets*, *122*, 295–328. https://doi.org/10.1002/2016JE005195

Singer, R. B. (1985). Spectroscopic observation of Mars. *Advances in Space Research*, *5*(8), 59–68.

Smits, F., & Gentner, W. (1950). Argonbestimmungen an kalium-mineralien I. Bestimmungen an tertiären kalisalzen. *Geochimica et Cosmochimica Acta*, *1*(1), 22–27. https://doi.org/10.1016/0016-7037(50)90005-6

Stack, K., Grotzinger, J., Kah, L., Schmidt, M., Mangold, N., Edgett, K., … Wiens, R. (2014). Diagenetic origin of nodules in the Sheepbed member, Yellowknife Bay formation, Gale Crater, Mars. *Journal of Geophysical Research: Planets*, *119*, 1637–1664. https://doi.org/10.1002/2014JE004617

Sunshine, D. (2010). Mars Science Laboratory CHIMRA: A device for processing powdered Martian samples, *Technical Report for NASA*.

Sutter, B., McAdam, A., Mahaffy, P., Ming, D., Edgett, K., Rampe, E., … Grotzinger, J. (2017). Evolved gas analyses of sedimentary rocks and eolian sediment in Gale Crater, Mars: Results of the Curiosity rover's sample analysis at Mars (SAM) instrument from Yellowknife Bay to the Namib dune. *Journal of Geophysical Research: Planets*, *122*. https://doi.org/10.1002/2016JE005225

Swindle, T., Treiman, A., Lindstrom, D., Burkland, M., Cohen, B., Grier, J., … Olson, E. (2000). Noble gases in iddingsite from the Lafayette meteorite: Evidence for liquid water on Mars in the last few hundred million years. *Meteoritics & Planetary Science*, *35*(1), 107–115. https://doi.org/10.1111/j.1945-5100.2000.tb01978.x

Thomson, B., Bridges, N., Milliken, R., Baldridge, A., Hook, S., Crowley, J., … Weitz, C. (2011). Constraints on the origin and evolution of the layered mound in Gale Crater, Mars using Mars Reconnaissance Orbiter data. *Icarus*, *214*(2), 413–432. https://doi.org/10.1016/j.icarus.2011.05.002

Treiman, A. H. (2005). The nakhlite meteorites: Augite-rich igneous rocks from Mars. *Chemie der Erde-Geochemistry*, *65*(3), 203–270. https://doi.org/10.1016/j.chemer.2005.01.004

Treiman, A. H., & Filiberto, J. (2015). Geochemical diversity of shergottite basalts: Mixing and fractionation, and their relation to Mars surface basalts. *Meteoritics & Planetary Science*, *50*(4), 632–648. https://doi.org/10.1111/maps.12363

Treiman, A. H., Bish, D. L., Vaniman, D. T., Chipera, S. J., Blake, D. F., Ming, D. W., … Yen, A. (2016). Mineralogy, provenance, and diagenesis of a potassic basaltic sandstone on Mars: CheMin X-ray diffraction of the Windjana sample (Kimberley area, Gale Crater). *Journal of Geophysical Research: Planets*, *121*, 75–106. https://doi.org/10.1002/2015JE004932

Vaniman, D., Bish, D., Ming, D., Bristow, T., Morris, R., Blake, D., … Spanovich, N. (2014). Mineralogy of a mudstone at Yellowknife Bay, Gale Crater, Mars. *Science*, *343*(6169), 1243480. https://doi.org/10.1126/science.1243480

Vasconcelos, P. M., Brimhall, G. H., Becker, T. A., & Renne, P. R. (1994). $^{40}Ar^{39}Ar$ analysis of supergene jarosite and alunite: Implications to the paleoweathering history of the western USA and West Africa. *Geochimica et Cosmochimica Acta*, *58*(1), 401–420. https://doi.org/10.1016/0016-7037(94)90473-1

Vasconcelos, P., Farley, K., Malespin, C., Mahaffy, P., Ming, D., McLennan, S., … Rice, M. S. (2016). Discordant K-Ar and young exposure dates for the Windjana sandstone, Kimberley, Gale Crater, Mars. *Journal of Geophysical Research: Planets*, *121*, 2176–2192. https://doi.org/10.1002/2016JE005017

Wolff-Boenisch, D., Gislason, S. R., Oelkers, E. H., & Putnis, C. V. (2004). The dissolution rates of natural glasses as a function of their composition at pH 4 and 10.6, and temperatures from 25 to 74°C. *Geochimica et Cosmochimica Acta*, *68*(23), 4843–4858. https://doi.org/10.1016/j.gca.2004.05.027